EFDA–JET–PR(09)24

Suk-Ho Hong, A. Murari, T. Loarer, A. Huber, C. Grisolia, P. Monier-Garbet,
J. Winter and JET EFDA contributors

Evidence of a Pathway to Hydrocarbon Nanoparticle Formation in Fusion Plasmas and its Impact on Tritium Inventory

Evidence of a Pathway to Hydrocarbon Nanoparticle Formation in Fusion Plasmas and its Impact on Tritium Inventory

Suk-Ho Hong[1], A. Murari[2], T. Loarer[3], A. Huber[4], C. Grisolia[3], P. Monier-Garbet[3], J. Winter[5] and JET EFDA contributors*

JET-EFDA, Culham Science Centre, OX14 3DB, Abingdon, UK

[1]National Fusion Research Institute, 113 Gwahangno, Yusung-Gu, Daejeon, 305-333, Korea
[2]Association EURATOM-ENEA per lla Fusione. Consorzio RFX, 4-35127 Padova, Italy
[3]EURATOM-CEA/Cadarache, IRFM, F-13108 Saint-Paul-lez-Durance, 13108 France
[4]Forschungszentrum Jülich GmbH, Association EURATOM-FZ Jülich, Institut für Plasmaphysik, Trilateral Euregio Cluster, D-52425 Jülich, Germany
[2]Institute for Experimental Physics II, Ruhr-University Bochum, D-44780 Bochum, Germany
** See annex of F. Romanelli et al, "Overview of JET Results",*
(Proc. 22 [nd] IAEA Fusion Energy Conference, Geneva, Switzerland (2008)).

Preprint of Paper to be submitted for publication in
Nuclear Fusion

ABSTRACT.
The first observations of dense HydroCarbon Clouds (HCCs) in JET divertor are reported. They confirm the existence of plasma grown nanoparticles in JET plasmas. Due to their low temperature, high density, and high recombination rate, high density plasmas, detached configurations and MARFEs present favorable conditions for the formation of hydrocarbon molecules and hydrocarbon nanoparticles. These HCCs, identified with the new wide angle InfraRed (IR) camera, are always present during strong deuterium fuelling. The implications of these hydrocarbon nanoparticles for tritium inventory are estimated which can be very significant for ITER. The HCCs are also clearly visible in the high density phases leading to the formation of MARFE instabilities and they appear at least a second before the density limit disruptions caused by these instabilities. Therefore, the observation of HCCs in the divertor region can be a very useful indicator to predict density limit disruptions and can therefore contribute to alleviate a major issue for the operation of ITER.

1. INTRODUCTION

Fusion plasmas are confined by strong magnetic fields and heated by powerful auxiliary systems, leading to densities of about $10^{20}\,m^{-3}$ and temperatures of about 10keV. The parameter space of a Tokamak is limited on the one hand by operational constraints linked to safety and on the other hand by the stability properties of the plasma. With regard to the safety issues, one of the most severe constraints in the next machine, ITER, will certainly be the Tritium (T) inventory. The maximum amount of tritium in the device is subject to regulatory limits and therefore it has to be kept under control. As far as the machine protection is concerned, disruptions remain one of the major issues for the integrity of any machine and they will pose a particularly severe threat in ITER. Disruptions are abnormal terminations of the plasma due to instabilities caused by various reasons. Operation at high density is particularly dangerous in this respect. On the other hand high density is advantageous not only from the point of view of the energy production but also to reduce the severity of the plasma wall interactions. Indeed, operation at high plasma densities tends to reduce the edge temperature of the plasma and decrease the severity of the Edge Localised Modes (ELMs), which can have a strong impact on the first wall erosion. Therefore high density scenarios are considered essential to guarantee enough longevity of metallic walls like ITER's.

In this paper, we report the first observations of dense HydroCarbon Clouds (HCCs) obtained with InfraRed (IR) imaging of JET divertor during high density operation, meant to study disruptions. They confirm the existence of plasma grown nanoparticles in JET plasmas and complement the evidence obtained during the inspection below the divertor in 1999. During the strong deuterium fuelling phase (several seconds long) in these shots, instabilities called MARFEs (Multifaceteted Asymmetric Radiation From the Edge) are formed which are clearly visible in the IR images. Then the plasma detaches from the target divertor and disruptions normally follow. Once MARFEs are formed, their characteristics - low temperature ($T_e \sim 1$ eV), high density ($n_e \sim 10^{20}\,m^{-3}$, and high recombination rate ($\sim 10^{22}\,s^{-1}$) [1] —may trigger the production of higher hydrocarbon molecules

[2]. If a certain amount of carbon impurities per unit volume is present in the MARFE region, hydrocarbon nanoparticles can be formed. This process is very important and has to be carefully assessed since hydrocarbons can augment the retention of tritium, which is trapped in these nanoparticles in significant amounts. ITER indeed is expected to operate at edge plasma parameters close the ones leading to MARFEs in JET ($T_e \sim 1$eV and $n_e \sim 10^{20}\,m^{-3}$). Therefore it is extremely important to understand the details of the processes leading to the formation of hydrocarbons and nanoparticles so that the tritium retention can be properly kept under control in ITER. Another important aspect, on which the presented analysis could have an impact, is the understanding of the eroded material migration. The transport of hydrocarbons, both in normal operation and during disruptions, might contribute significantly to redeposition of the codeposited layers on the wall. During the MARFE formation, MARFEs are located mostly at the High Field Side (HFS) inner divertor region, thus they could contribute to explain the presence of the observed thick codeposited layers on inner divertor leg in JET [3].

The detection of hydrocarbon nanoparticles with IR cameras can have an impact also on disruption prediction. Disruptions are a concern for the next fusion machine ITER, because they cause high power loads on the plasma facing components and electromagnetic forces on the machine structures. The sudden energy losses accelerate the erosion of the wall materials, whereas mechanical stresses can induce leaks in the vacuum vessel or even more fundamental structural damages to the coils or vacuum vessel. Therefore, in order to reduce the potential risks, the number of disruptions during Tokamak operation has to be minimized. This requires a robust in situ disruption detection and warning system. On the other hand, the development of reliable disruption predictors has proved to be elusive for many years. In the case of high density operation, which will be routine in the next step device, hydrocarbon nanoparticles can be formed well in advance of the disruption occurrence and therefore they could become important indicators of the approach of dangerous situation.

Furthermore, this issue can constitute a link between the communities of low temperature dusty plasmas and of fusion plasmas, motivating interesting collaboration and cross-fertilization.

2. DIRECT OBSERVATION OF HYDROCARBON CLOUDS WITH JET WIDE ANGLE IR CAMERA

In JET as in the other major Tokamaks, when the density limit is approached, in many cases MARFEs occur. MARFEs are well known and intensively studied phenomena in various fusion machines [4]. They are considered as volume recombination zones characterized by low temperature, high density, and high recombination rate [1, 5]. If MARFEs are not properly suppressed or relaxed, disruptions are very likely. MARFEs can occur in a wide range of densities (e.g., $n/n_G \approx 0.4$-1), but they are much more likely just below the density limit [4].

In JET, density limit disruptions can be triggered by injecting deuterium in the divertor region. When the deuterium is continuously and strongly puffed, the radiation in the divertor increases and a MARFE is formed. The plasma then detaches from the target tiles and finally a major disruption

occurs. During the study of density limit disruptions (e.g. JET Pulse No's: 69327, 69343 and 70568-70584), the MARFE is clearly observed by visible (fast CCD) and IR cameras, and by bolometry.

The original aim of the IR camera installed on JET is to measure the blackbody radiation from the Plasma Facing Components (PFCs) in order to calculate the temperature and the total heat power loads on the first wall. JET IR camera is installed on a wide angle viewing endoscope. The observation range is between 3.6-5.1μm with two optical filters at wavelengths of 3.97-4μm and at 4.2-4.4μm. Figure 1 shows images measured by the IR wide angle camera and the radiated power reconstruction from bolometry at different times corresponding to the MARFE formation, during the density limit disruption studies (from JET Pulse No: 69331). Fig.1(a) shows the MARFE observed in the divertor region (partially detached), Fig.1(b) and (c) are frames after the plasma has completely detached. It is very interesting that the MARFEs emit large amount of photons in the IR range, for several seconds. In general, IR temperature measurements assume that the plasma itself is not a significant source of IR radiation. Nevertheless, it is appropriate that, in the discharges considered, the IR radiation is not due to the bremsstrahlung continuum. The bremsstrahlung emission can be expressed as

$$\frac{\Delta P}{\Delta \lambda} = \frac{-1.89\times10^{-28}\, n_e^2 Z_{eff}\, g_{eff}}{T_e^{1/2}\, \lambda^2} \exp\left(\frac{-12400}{\lambda}\right)$$

where $Z_{eff} = \Sigma n_e Z_i^2 / n_e$ the wavelength λ is in Å , the electron density n_e is in cm^{-3}, the electron temperature Te is in eV and the temperature-averaged free-free Gaunt factor is expressed as g_{ff} = 1.35 15 . 0 e T [6]. The calculations of the Bremstrahlung emission, in the parameter region of interest for the considered discharges i.e. with Te~1 eV and $n_e \sim 10^{20}\, m^{-3}$ compared with calculations for "normal" edge temperatures of T_e~ 40-70 eV at $n_e \sim 10^{20}\, m^{-3}$, show that the increase of the bremsstrahlung is proportional to n^2_e for wavelengths up to 0.6μm then it decreases rapidly in the longer wavelength range (see Figure 2). The bremsstrahlung at 4m is an order of magnitude smaller than that at 0.6μm. This indicates that, if bremsstrahlung radiation was detected even in the IR range in a shot, the visible bremstrahlung in that shot would have to be much more intense than that of shots without the IR signature. This is not the case in JET where the visible bremsstrahlung is far too low to be compatible with the emission in the IR. Moreover, the time evolutions of the IR radiation and visible radiation are also very different. Figure 3 shows visible bremsstrahlung measurements (at 523nm) (a) measured by a vertical camera which covers the whole divertor area and (b) at the outer divertor during the density limit experiments. See table 1 for more information on the plasma operation parameters. The MARFEs are observed by the IR camera in the Pulse No's: 69331 and 70578 (with deuteruim puffing), but not in the Pulse No's: 69335 and 69339 (without deuterium puffing). The bremsstrahlung signals without deuterium fuelling show almost the same tendency and amplitude in both vertical and outer divertor, whereas the bremsstrahlung signals with deuterium fuelling show a much higher increase in the outer divertor. Since the MARFE is located on the high field side as observed by IR images and bolometry (see Fig.1), the increase of

bremsstrahlung signal in the outer divertor cannot be ascribed directly to the MARFE. Furthermore, the visible bremstrahlung level is much higher in the Pulse No: 69335 than that in Pulse No: 70578, but no MARFE-like radiation in IR range is observed in the Pulse No: 69335. A direct evidence indicating that the IR radiation cannot be due to bremsstrahlung emission, is also Pulse No: 70578 with the modulation of the deuterium puffing. Note that, the IR images of this shot are taken by using the 4.2-4.4μm optical filter. The modulation is seen by visible bremsstrahlung in Fig.3. Although the net change in the bremsstrahlung level (ΔP_{Br}) is much smaller compared with the other shots in Fig.3, the formation/relaxation of the MARFE is clearly observed by the IR camera as the deuterium puffing is turned on and off. Thus, if ΔP_{Br} is enough to contribute to the observed IR radiation in the case of such low visible bremsstrahlung, such IR radiation should to be present always in all JET shots and this emission would jeopardize the measurement of the plasma facing components temperature from IR thermography, which on the contrary is routinely available in JET.

On the other hand, hydrocarbons are known to have a strong IR emission/absorption feature, around 3.4μm-3.6μm [aliphatic C-H stretch and polycyclic aromatic hydrocarbons (PAHs)] [7], strong C-D stretch around 3.8μm-4.5μm, as listed in table 2 [8]. Figure 4 shows the C-H and C-D IR bands in the wavelength range detected by JET IR camera. It is clear that many hydrocarbon IR bands exist in the detected interval and such hydrocarbon emission may contribute significantly to the IR measurements [9] especially when their density is high enough. Indeed, a large amount of hydrocarbons in MARFEs and detached plasmas are also observed in TEXTOR-94 by emission spectroscopy and mass spectrometry [2, 10], which support the IR observations described above. From the evidence discussed above, the observed radiation in IR images cannot be attributed to the bremsstrahlung continuum in the IR range, but it is likely that a large amount of hot hydrocarbon species (including hot hydrocarbon nanoparticles, see below) are concentrated in the MARFE and form observable “clouds” emitting also in the infrared part of the spectrum.

It is also worth mentioning that, the sequential processes shown in Figure 1 indicate another hydrocarbon transport mechanism in the vacuum vessel, which might contribute the redeposition of hydrocarbons on the HFS inner divertor leg and vessel walls. Moreover, even if the dynamic of these phenomena will have to be studied in more detail to understand the details, it is very clear that the detection of the hydrocarbon clouds and their displacements in the divertor region can be used as very early indicators of the imminence of disruptions. Indeed this IR radiation due to hydrocarbons is observable even 1-2 seconds before the density limit disruptions. The detection in realtime of the cloud formation will therefore be in the future one important element in the strategy to avoid high density disruptions and actions are in place at JET to include fast image processing of the IR camera to implement this disruption prediction technique in the near future.

3. A POSSIBLE PATHWAY TO NANOPARTICLE FORMATION IN FUSION PLASMAS

Figure 5 shows a Scanning Electron Microscopy (SEM) picture of dusts showing nanoparticles collected at JET after the DTE1 campaign [27], with measured radius profile of the nanoparticles.

The nanoparticle size and their number density are determined by image processes developed at Tore Supra. Two different particle sizes are identified: a Gaussian fit of the curves shows a broad range of small size nanoparticles (r<40 nm) and a group of nanoparticles of bigger size centered at about 57nm with a FullWidth-Half-Maximum (FWHM) of 25nm. About 1475 nanoparticles were identified in 7.75×10^{11} m^{-2}, which gives particle number densities of 1.125×10^{13} m^{-2} for r = 57nm particles and 7.78×10^{12} m^{-2} for smaller particles. Note that, the nanoparticle size distribution with a well defined Gaussian shape within a certain FWHM constitutes a clear evidence of plasma volume polymerization [11]. Other dust creation processes like arcing, brittle destruction, or flaking of redeposited layers never give such a particle size distribution with spherical shape. This reveals that a parameter window for nanoparticle formation exists, even in fusion plasmas, with sufficient amount of hydrocarbons exceeding the critical density for the initiation of the process. Assuming toroidal symmetry of the nanoparticle formation, a deposition surface area of the plasma facing components of $\approx10m^2$ (a realistic estimation for JET Mk-I divertor [12]), and a nanoparticle density of $1.6g/cm^3$, then the Specific Surface Area (SSA) of these nanoparticles in Fig.5 is about $32.89m^2/g$, which is comparable with measured SSAs in JET ($4\text{-}36.4m^2/g$) [13].

How such nanoparticles can be formed in fusion devices? The surface of an object immersed in a plasma experiences both deposition and erosion. Depending on the plasma parameters, the dominant process governs the net interaction. Under standard discharge conditions in fusion devices, dusts in the plasma experience net erosion. According to recent modelling works [14], however, in some cases (e.g., detached divertor plasmas, afterglow plasmas after discharge termination or disruption, and parasitic plasmas that occur in "shadow" regions in some tokamaks), the dusts can grow when a low temperature plasma contains significant concentrations of intrinsic impurities. In the parameter region of T_e below 10eV and ne in the range $10^{18}\text{-}10^{20}$ m^{-2}, assuming 1% of carbon ion impurity fraction in deuterium plasma, dusts may grow with a maximum growth rate of 100nm/s and they survive as long as the plasma pulse duration, i.e. of the order of seconds. Carbon neutrals can increase the growth rate and render the growth region wider [14].

If we compare the plasma parameter region for the dust growth in fusion plasmas suggested by Smirnov et al [14] (see Table 3), it is overlapping with typical MARFE characteristics. The MARFE study in TEXTOR-94 indicates that the carbon is the major source of the MARFE formation [10]. In W7-AS, MARFEs have been observed by IR and visible spectroscopy for $D\alpha$, $D\gamma$ and C_{II} [15]. They found that the MARFE has some kind of structure which consists of a low temperature deuterium core surrounded by a carbon shell. In JET, the increase of CII emission above the inner strike point is detected by divertor camera after the plasma detaches from the inner divertor [5]. Investigations on MARFEs in many machines, including JET, indicate abundance of carbon impurities in the MARFE regions [5, 10, 15]. From the impurity study in TEXTOR- 94, Philipps et al found about 1.5%-4% of carbon impurities with "old" boronized wall conditions. These C2-yields are dominated by hydrocarbons ($C_2D_xH_y$) such as acetylene (x + y = 2) and ethane (x + y = 4), which increase as plasma density increases or as temperature decreases (maximum at detached

plasma) [2]. Similar overall hydrocarbon formation rates were observed by mass spectroscopy in the divertor exhaust of ASDEX Upgrade [16]. These indicate that hydrocarbon impurities in the MARFE region undergo chemical process to form higher hydrocarbons. Note that the C_2H- radical from the reaction

$$C_2H_2 + e^- \rightarrow C_2H^- + H$$

is considered the starting point of hydrocarbon nanoparticle formation in low temperature hydrocarbon dusty plasmas [11, 17]. It is also reasonable to expect that the low temperature (T_e ≈1eV) of MARFEs can enhance the survival time of hydrocarbons, which causes further growth of nanoparticles up to nanometer size. Moreover from astrophysical studies, it is known that such dust particles (about 10nm size) are heated by the ambient radiation field and emit thermally in the IR range [18]. Smirnov et al [14] have suggested, on the basis of quite accurate calculations, that the temperature of dusts in the growth zone may be higher than 1000 K, which can be seen directly by IR cameras.The carbon chemical bonding structure of nanoparticles, found in Tore Supra neutralizer (r<30nm), confirms that they have been exposed to temperatures higher than 1000°C [19]. Furthermore, calculations for low temperature acetylene plasmas indicate that the number densities of hydrocarbon species (ions and radicals), leading to nanoparticle formation, are of the order of 10^{15}-10^{16} m^{-3} [17]. These values are close to the parameter range suggested by Smirnov et al., but with somewhat lower electron density of 5×10^{14} m^{-3}. Table 3 reports a summary of the parameter ranges described above.

To summarize, collected dusts in fusion devices (e.g., in JET as shown in Fig.5, in Tore Supra neutralizer [19]), constitute quite strong evidence for the suggested pathway to hydrocarbon nanoparticle formation, although the detailed mechanisms have not been experimentally proven yet [20]. The IR observations of MARFEs described in this paper provide new support to the phenomenon, since they show the presence of these particles in the divertor of JET during high density discharges. Further investigations of the detailed mechanisms leading to the formation of hydrocarbon nanoparticles are appropriate and are expected to be of common interest for both communities of low temperature dusty plasmas and fusion edge plasmas.

4. TRITIUM RETENTION ISSUES DUE TO NANOPARTICLES

Assuming that the MARFE region is the birth place of hydrocarbon nanoparticles found in fusion devices, a very reasonable hypothesis as shown in the previous sections, it is interesting to calculate possible T inventory rates of hydrocarbon nanoparticles. The size of a MARFE can be evaluated by using $n_i/n_e \geq 1/\Delta_2$ [21], where Δ is the width of the MARFE, n_i and n_e represent impurity and electron density, respectively. The equation gives a MARFE width up to 10cm for typical edge plasma parameters in JET, $n_e = 3\times10^{19}$ m^{-3} and $T_e = 20$eV with impurity fraction of $n_i/n_e = 0.01$. The average pixel size of a MARFE cross-section in JET IR images, just before detachment [Fig.1(b)],

is about 30 pixels. 1 pixel corresponds to 15mm × 15mm, which gives an area of 67.5cm^2. Assuming a MARFE of circular shape, a radius of r_t = 4.64cm is obtained, which is consistent with the above MARFE size calculation. The volume of a "MARFE torus" in JET is then 1.04×10^5 cm^3. For a fully detached MARFE of an average value of 640 pixels [Fig. 1 c)], an area of 1.44×10^3 cm^2 is obtained, which gives r_t = 21.41cm, thus a volume of 2.37×10^6 cm^3 is obtained.

In order to calculate the tritium inventory rate in nanoparticles, the size dependent characteristics of individual nanoparticles have to be considered. Recent investigations of a-C:H nanoparticles, prepared in Ar-CH_4 and Ar-C_2H_2 low temperature dusty plasmas by Hong et al [22, 23], indicate that a-C:H nanoparticles have a so called "core-shell" internal structure with different complex refractive indices, meaning different hydrogen to carbon ratio: very high refractive index in the core, a refractive index similar to graphite-like materials (m = 1.96−0.125i) in the first shell, then a refractive index similar to soft polymer-like materials (m = 1.55−0.02i) The internal structure of nanoparticles assumed for the tritium inventory calculation is shown in Table 4. The physical parameter responsible for the change of the refractive index as a function of particle size is the temperature of nanoparticles. The smaller the particle size is, the higher the particle temperature is. As their size increases, the particle temperature decreases [28]. This leads to the hydrogen reduction at smaller radii resulting in different hydrogen to carbon ratios as a function of particle size. Since the refractive index of hydrocarbon materials is a quasi direct indicator of carbon contents [24], it is possible to deduce the hydrogen to carbon ratio from the refractive indices of the materials. Comparing with known hydrocarbon materials of similar refractive indices, H/C ratios of 0.4-0.6 in the graphitelike shell and H/C>1 in polymer-like shell are derived. The following calculations provide an estimate of the tritium inventory per nanoparticle formation event (MARFElike event) with nanoparticle structures shown in Table 4. Assuming that a particle has a core of 25nm in radius (no hydrogen with the density of graphite, i.e. 2g/cm^3) and two sequential shells, i.e. 25<r<50 nm "graphite-like", carbon density of 1.6g/cm^3 with (D+T)/C ratio of 0.4, and T/D ratio of 1 (since the D:T ratio in gas phase in fusion is 1), simple calculations lead to an upper limit of a tritium inventory value of 3.67×10^{-17}g/particle. Since the volume polymerization process occurs only when a critical density of precursor is present, typical number density of hydrocarbon nanoparticles in low temperature dusty plasmas, nd=108/cm3 is also assumed as a lower limit. For larger particles, different (D+T)/C ratio has to be considered for the second shell, typically a density of 1.0g/cm^3 with (D+T)/C ratio of 1.

The summary of the calculated tritium inventory for a MARFE of radius rt=4.64cm is shown in Table 5. The total amount of carbon and tritium atoms in nanoparticles, the T/C atomic/weight ratio and the Specific Surface Area (SSA) are reported. The deuterium mass is also considered in the Specific Surface Area (SSA) calculation. If nanoparticles have a radius of 25 nm, the total number of carbon atoms in the 1.04×10^{13} nanoparticles of the assumed MARFE are 6.79×10^{19} which is equal to 1.36mg. The specific surface area (SSA) of nanoparticles is 60.29m^2/g. At a radius of 50nm (similar size as shown in Fig.5), 4.48×10^{19} (8.98mg) C atoms and 7.61×10^{19} (0.38mg) T

atoms would be present in the nanoparticles. The T/C atomic ratio is 0.17, the T/C weight ratio is 0.04, and the SSA is 34.34m^2/g. Larger particles, e.g., at a radius of 100nm, have 2.35×10^{21} (47 mg) C atoms and 1.03×10^{21} (5.16mg) T atoms with T/C atomic ratio of 0.44, T/C weight ratio of 0.11, and SSA of 23.52 m^2/g. Remember, these numbers represent tritium inventory and the increase of the SSA per MARFE-like event. Scaling up the MARFE torus volume in JET to that in ITER, a value of 5.62 x 105 cm3 is obtained (volume fraction of 5.4), thus the upper limits of the tritium inventory per MARFE-like event in ITER are 2.06mg for particles of radius r = 50nm, and 28.1mg for r = 100nm (Table 6). For nanoparticles found after DTE1 campaign in Fig. 5, a total tritium inventory of 4.13mg is obtained by applying calculated tritium inventory value of 3.67 x 10-17 g/ particle (r = 50nm) to the particle number density 1.125×10^{13} m^{-2} on 10m^2 surface area. If nanoparticles of the same size as in DTE1 campaign (Fig.5) are formed in ITER (x10 of surface area), 41.3mg of tritium in total will be present in the nanoparticles.

It is important to mention that tritium retention in nanoparticles must not be confused with that in dusts and flakes. Usually, dusts are defined as mobilized flakes originated from layers codeposited on surfaces. Flakes have experienced sequential heating and cooling repeatedly during their lifetime, depending on their in-vessel location. Once their surface layer is heated over 300-400^{o}C, hydrogen reduction starts due to thermal desorption. Thus, depending on their heating/cooling history and the in-vessel position from where flakes are located, the inventory rates of hydrogen isotopes in dusts vary significantly, sample by sample. On the other hand, it has to be emphasized that the ITER divertor operation regimes [25] indicate that the plasma parameters in the divertor region are very similar to the parameters used above to calculate the tritium content of hydrocarbon nanoparticles, i.e., $T_e \approx 1$eV, $n_e \approx 10^{20}$ m^{-3}, and detachment is considered as the routine mode of operation to reduce heat loads on the divertor plates. Note that, in detached or afterglow plasmas, a particle growth rate of 1 •m/s is obtained from model calculations for $T_e \approx 3$eV, $n_e \approx 10^{20}$ m^{-3} with 1% of carbon ion impurity fraction [26].

Furthermore, long pulse lengths in these conditions may enhance the survival time of the nanoparticles, thus enlarging the particle size. For a nanoparticle of 500nm in radius, the upper limit of the T inventory of 3.67g per second per MARFE-like event (see Table 6) even without disruptions. Moreover, as we have shown above, nanoparticles would provide much large specific surface area to tritium for further potential retention. Therefore, diagnostics to systematically investigate hydrocarbon nanoparticles in existing fusion devices have to be urgently developed and deployed in order to assess their potential impact on tritium inventory in ITER.

CONCLUSIONS AND FUTURE PROSPECTS

Clear evidence of dense hydrocarbon clouds in JET divertor has been collected using JET wide angle IR camera in high density experiments aimed at studying disruptions. Such dense hydrocarbon clouds are known to lead to hydrocarbon nanoparticle formation in the parameter space accessed during the discharges to study disruptions. Therefore at least a part of the IR emission is expected

to be the thermal IR radiation from these hot hydrocarbon nanoparticles. Therefore, the IR observations are expected to shed some light on the formation mechanism of these nanoparticles in fusion plasmas, which have not been explained yet. Moreover, since the existence of such hydrocarbon nanoparticles will affect the tritium inventory in ITER, it is important to avoid the regimes of operation in which their rate of formation can pose a problem. It has also to be emphasised that systematic investigations of nanoparticles observed in fusion devices are urgent, to understand both the creation process and the possible removal methods. JET is the most suited machine to investigate these issues, at the plasma parameters closets to ITER, with the present carbon divertor and in the future with a completely metal first wall.

ACKNOWLEDGEMENTS

Authors thank Glenn Counsell, Mike Stamp, and Sandrine Rosanvallon for valuable discussions and helpful comments on the manuscript. This work, supported by the European Communities under the contract of Association between EURATOM and CEA, was carried out within the framework of the European Fusion Development Agreement. The views and opinions expressed herein do not necessarily reflect those of the European Commission.

REFERENCES

[1]. B. Lipschultz, J.L. Terry, C. Boswell, A. Hubbard, B. LaBombard, and D.A. Pappas, "Ultrahigh densities and volume recombination inside the separatrix of the Alcator CMod tokamak", Phys.Rev. Lett., **81**(5):1007-1010, Aug 1998

[2]. V. Philipps, A. Pospieszczyk, H.G. Esser, U. Ktigler, G. Mank, U. Samm, B. Schweer, J. von Seggern, B. Unterberg, E. Vietzke, F. Weschenfelder, P. Wienhold, J. Winter, and the TEXTOR team, "Impurity release and deposition processes close to limiter surfaces in TEXTOR-94", Journal of Nuclear Materials, **241-243**:105-117, 1997

[3]. A.T. Peacock, P. Andrew, P. Cetier, J.P. Coad, G. Federici, F. H. Hurd, M.A. Pick, and C.H. Wu, "Dust and flakes in the JET MK-IIa divertor, analysis and results", Journal of Nuclear Materials, 266-269:423-428, 1999

[4]. M. Greenwald, "Density limits in toroidal plasmas", Plasma Physics and Controlled Fusion, **44** (8):R27-R53, 2002

[5]. G.M. McCracken, M.F. Stamp, R. D. Monk, A. G. Meigs, J. Lingertat, R. Prentice, A. Starling, R. J. Smith, and A. Tabasso, "Evidence for volume recombination in JET detached divertor plasmas", Nuclear Fusion, **38** (4):619-629, 1998

[6]. H. Yamazaki, S. Morita, M. Goto, K. Tanaka, and R. Sakamoto, "Application of visible bremsstrahlung to a density monitor in steady state fusion reactor", Fusion Engineering and Design, **81** (23-24):2817-2821, November 2006

[7]. G. Sokrates,"Infrared & Raman characteristic group frequencies: tables & charts", Wiley, 2004

[8]. National institute of science and technology database.

[9]. P. Andrew, J.P. Coad, T. Eich, E. Gauthier, A. Herrmann, G.F. Matthews, V. Riccardo, and M. Stamp, "Thermal effects of surface layers on divertor target plates", Journal of Nuclear Materials, **313-316**:135-139, 2003

[10]. G. Sergienko, A. Pospieszczyk, M. Lehnen, M. Brix, J. Rapp, B. Schweer, and P.T. Greenland, "Spectroscopic studies of stationary MARFEs in TEXTOR-94", Journal of Nuclear Materials, **290-293**:720-724, 2001

[11]. S. Hong, J. Berndt, and J. Winter, "Growth precursors and dynamics of dust particle formation in the Ar/CH4 and Ar/C2H2 plasmas", Plasma Sources Science and Technology, 12(1):46-**52**, 2003

[12]. M.J. Rubel, J.P. Coad, R.A. Pitts, and Contributors to the JET-EFDA Workprogramme, "Overview of co-deposition and fuel inventory in castellated divertor structures at JET", Journal of Nuclear Materials, **367-370**:1432, 2007

[13]. N. Bekris, J.P. Coad, R.-D. Penzhorn, S. Knipe, L. Doerr, R. Rolli, and W. Ngele, "Characterisation of flakes generated in JET after D-D and D-T plasma operations", Journal of Nuclear Materials, **337-339**:659-663, March 2005

[14]. R.D. Smirnov, A. Yu. Pigarov, M. Rosenberg, S.I. Krasheninnikov, and D.A. Mendis, "Modelling of dynamics and transport of carbon dust particles in tokamaks", Plasma Physics and Controlled Fusion, **49**(4):347-371, 2007

[15]. U. Wenzel, K. McCormick, D. Hildebrandt, S. Klose, D. Naujoks, and H. Thomsen, "Experimental observation of MARFEs in the W7-AS stellerator", Plasma Physics and Controlled Fusion, **44**(10):L57-L55, 2002

[16]. W. Poschenrieder, K. Behringer b, H.-St. Bosch, A. Field, A. Kallenbach, M. Kaufmann, K. Krieger, J. Kiippers, G. Lieder, D. Naujoks, R. Neu, J. Neuhauser, C. Garcia-Rosales, J. Roth, R. Schneider, and ASDEX UPGRADE-team, "Molecular impurities in ASDEX Upgrade plasma discharges", Journal of Nuclear Materials, **220- 222**:36-49, 1995

[17]. K. De Bleecker, A. Bogaerts, and W. Goedheer, "Detailed modeling of hydrocarbon nanoparticle nucleation in acetylene discharges", Physical Review E (Statistical, Nonlinear, and Soft Matter Physics), **73**(2):026405, 2006

[18]. B.T. Draine, "Interstellar dust grains", Annual Review of Astronomy and Astrophysics, **41**(1):241-289, 2003

[19]. P. Roubin, C. Martin, M. Richou, C. Pardanaud, Y. Marandet, B. Pgouri, C. Brosset, J. Gunn, and R. Smirnov, "Tore supra carbon deposited layers: characterization and growth process", In 18th International Conference on Plasma Surface Interactions, 2008

[20]. J. Winter, "Dust in fusion devices - experimental evidence, possible sources and consequences", Plasma Physics and Controlled Fusion, **40**(6):1201-1210, 1998

[21]. J. Wesson. Tokamaks. Oxford, 2004

[22]. S.-H. Hong and J. Winter, "Micro-raman spectroscopy on a-c:h nanoparticles", Journal of Applied Physics, **98**:4304, December 2005

[23]. S.-H. Hong and J. Winter, "Size dependence of optical properties and internal structure of plasma grown carbonaceous nanoparticles studied by in situ rayleigh-mie scattering ellipsometry", Journal of Applied Physics, **100**:4303, September 2006

[24]. T. Schwarz-Selinger, A. von Keudell, and W. Jacob, "Plasma chemical vapor deposition of hydrocarbon films: The influence of hydrocarbon source gas on the film properties", Journal of Applied Physics, **86**:3988-3996, October 1999.

Pulse No:	B_T(T)	I_P(MA)	P_{tot}(MW)
69331	1.7	1.5	10
69335	1.3	1.5	12.5
69339	0.95	1.5	8.2
70578	2.7	1.7	2.7

Table 1: Summary of plasma parameters of JET Pulse Numbers

Molecule	Mode	cm^{-1}	μm	JET IR filter (μm)
C_2D_4	CD a-Str.	2345	4.26	4.2-4.4
C_2HD	CD Str.	2584	3.92	3.97-4.0
C_2D		2537	3.94	
C_3D_2		2458	4.06	
C_3D_2		2482	4.03	

Table 2: Molecular C-D IR emission/absorption bands at JET IR filter wavelength ranges (3.97-4.0μm, 4.2-4.4μm).

parameter	Smirnov et al [14]	Detached plasmas and MARFEs [2, 5]	Low temperature dusty plasmas [17,28]
n^e (m^{-3})	10^{18}-10^{20}	10^{19}-10^{21}	10^{14}-10^{18}
C impurity (m^{-3})	10^{16}-10^{18}	10^{17}-10^{19}	10^{15}-10^{16}
T_e (eV)	<10	≈1	3-5

Table 3: Summary of plasma parameters of various "dusty"" plasmas.

Radius (nm)	Density (g/cm3)	(D+T)/C ratio	D/T ratio
25	2	0	0
50	1.6	0.4	1
100	1.0	1	1

Table 4: Assumed internal structure of nanoparticles for T inventory calculation according to Hong et al [21].

radius (nm)	C atoms (in total)	T atoms (in total)	atomic T/C	weight T/C	SSA (m^2/g)
25	6.79×10^{19} (1.36 mg)	0	0	0	60.29
50	4.48×10^{20} (8.98 mg)	7.61×10^{19} (0.38 mg)	0.17	0.04	34.34
100	2.35×10^{21} (47 mg)	1.03×10^{21} (5.16 mg)	0.44	0.11	23.52
500	2.71×10^{23} (5.43 g)	1.36×10^{23} (0.68 g)	0.5	0.13	4.98

Table 5: Calculated T inventory in nanoparticles per nanoparticle formation during a MARFE-like event in JET.

radius (nm)	C atoms (in total)	T atoms (in total)	atomic T/C	weight T/C	SSA (m^2/g)
25	3.67×10^{20} (7.35 mg)	0	0	0	60.29
50	2.42×10^{21} (48.54 mg)	4.11×10^{20} (2.06 mg)	0.17	0.04	34.34
100	1.27×10^{22} (254.53 mg)	5.61×10^{21} (28.1mg)	0.44	0.11	23.52
500	1.46×10^{24} (29.23 g)	7.24×10^{23} (3.67g)	0.5	0.13	4.98

Table 6: Calculated T inventory in nanoparticles per nanoparticle formation during a MARFE-like event in ITER.

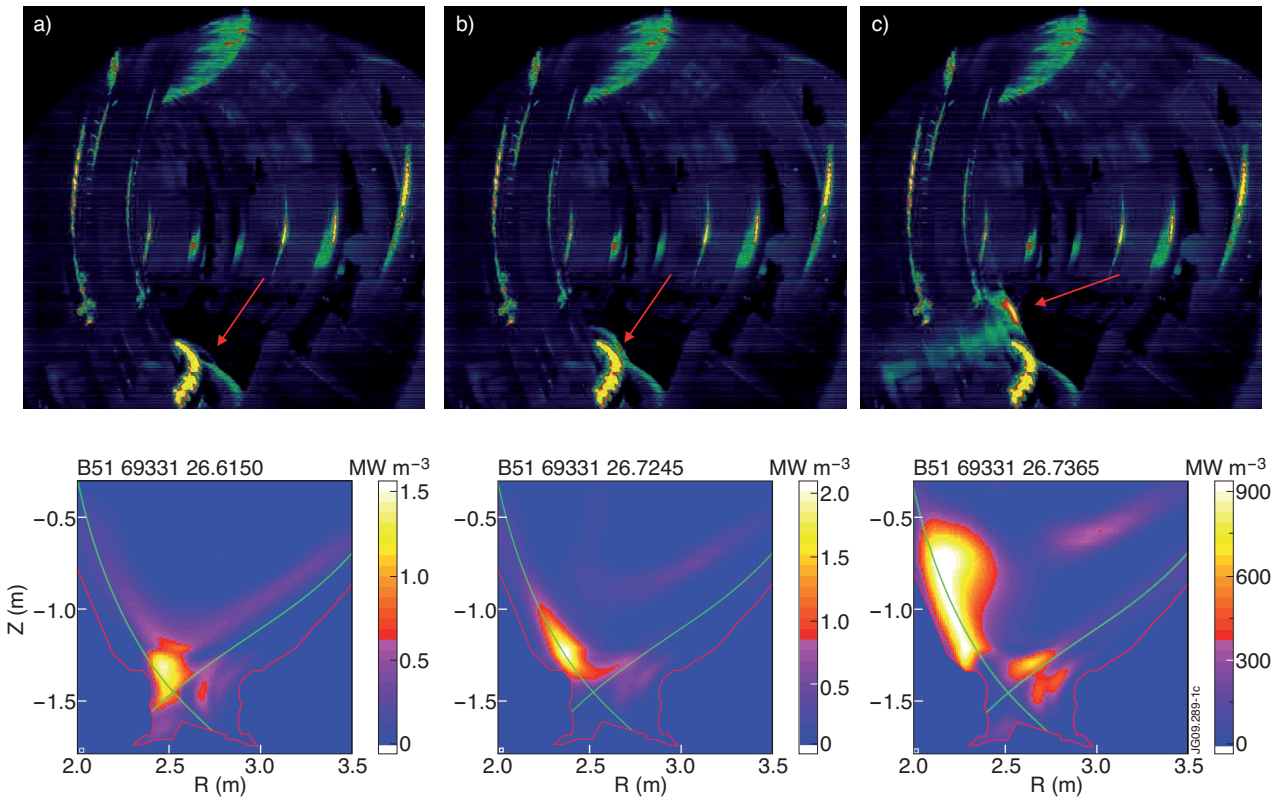

Figure 1: IR images with bolometric reconstructions of MARFEs during density limit disruptions. a) and b) show before and just after the plasma detachment, c) shows after the complete detachment.

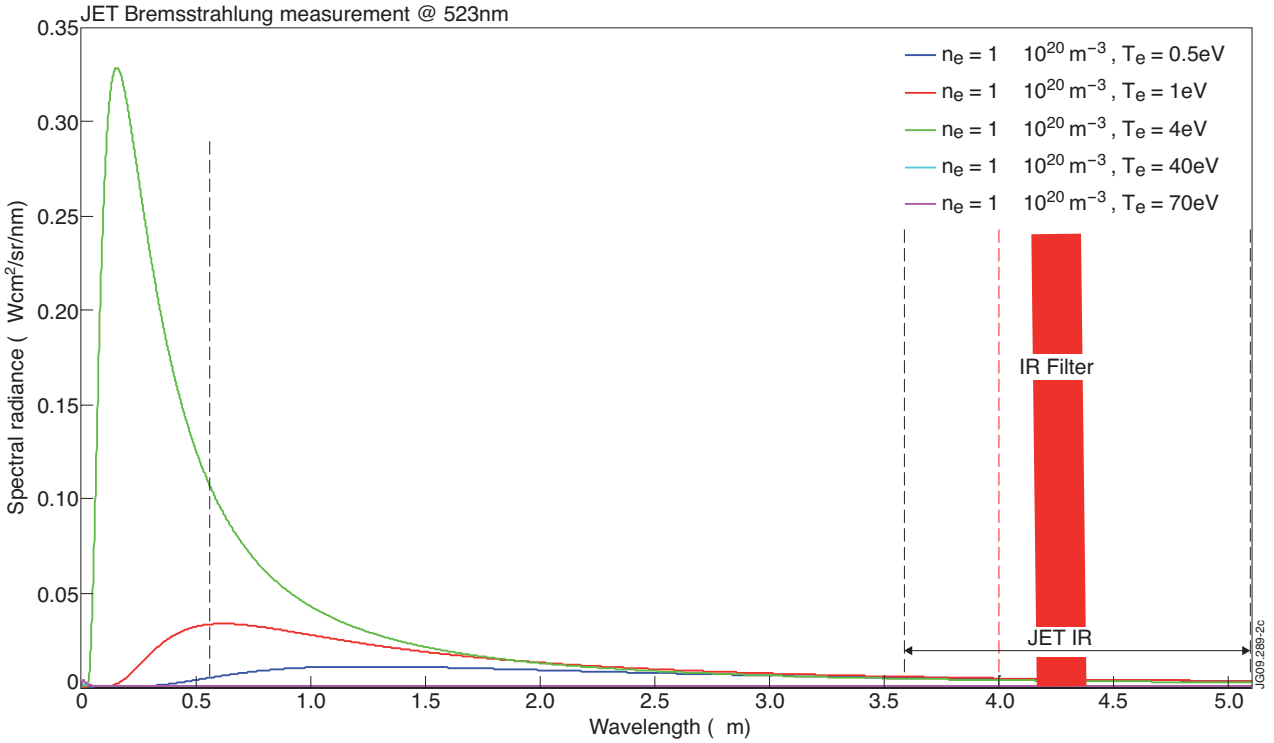

Figure 2: Calculated Bremsstrahlung with $T_e \sim 1eV$ and $n_e \sim 10^{20}\ m^{-3}$, compared with calculations for "normal"" edge temperatures of $T_e \sim 40\text{-}70eV$ at $n_e \sim 10^{20}\ m^{-3}$. JET IR camera range as well as IR filter locations are depicted.

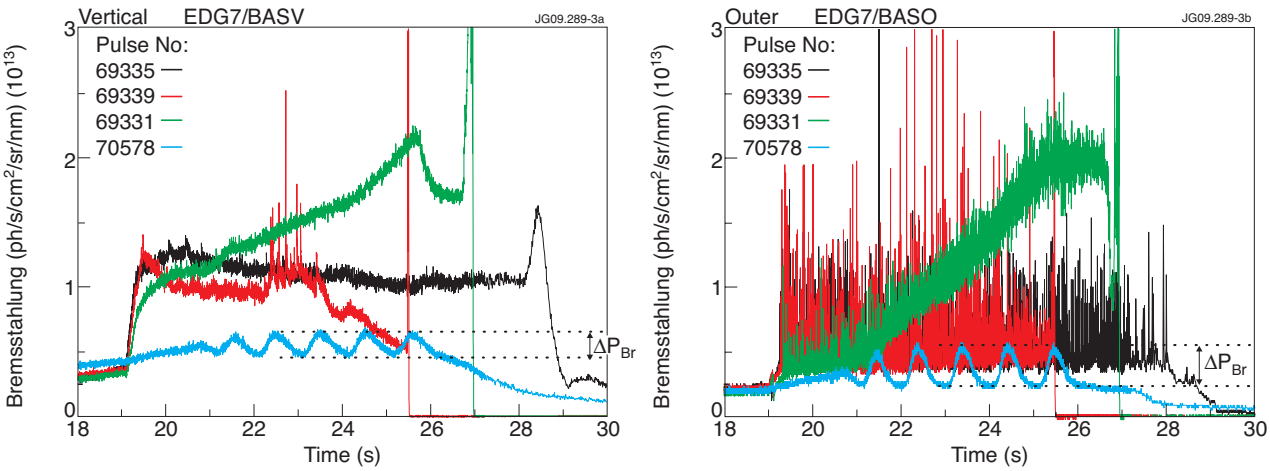

Figure 3: Measured visible bremsstrahlung radiations during the density limit disruption studies in JET. At 19 seconds, the neutral beam heating is turned on, thus the signal level increases. Deuterium fuelling starts at 21 seconds. a) measured by the vertical camera, b) in the outer divertor.

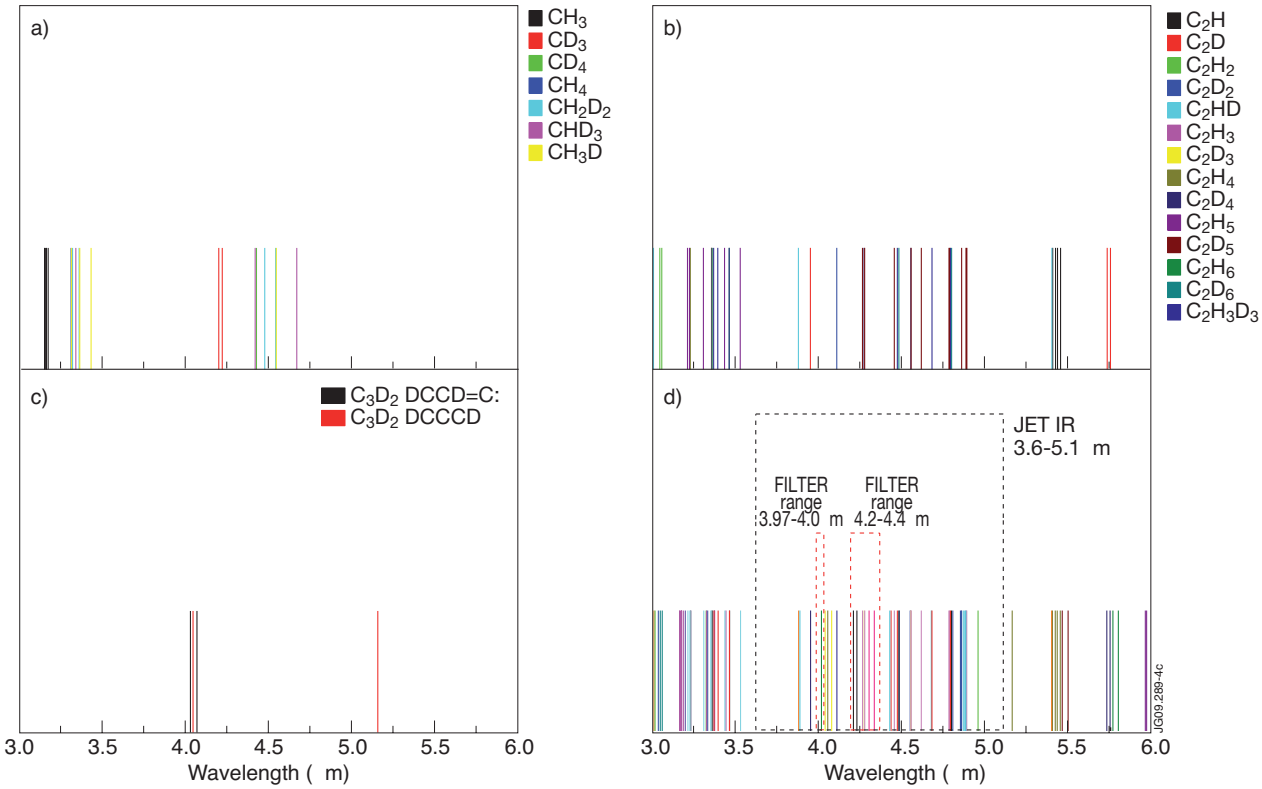

Figure 4. C-H, C-D IR bands in the range of 3.0μm to 5.5μm. a) CH_x and CD_y, b) C_2H_x and C_2D_y, c) C_3Hx and C_3D_y, d) overview of all bands with JET IR camera range and filter locations.

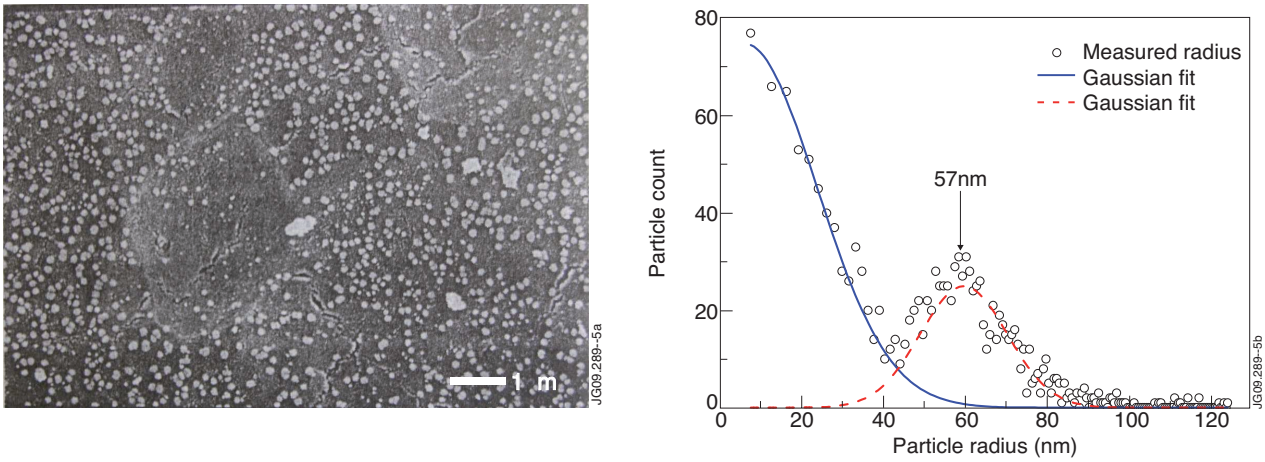

Figure 5: a) SEM picture of collected nanoparticles from JET after DTE1 campaign (adopted from Ref. [27]) b) particle size distribution obtained by image analysis.